

International Journal of Computational Materials Science and Surface Engineering

ISSN online: 1753-3473 - ISSN print: 1753-3465
<https://www.inderscience.com/ijcmsse>

A finite element simulation for notch stress intensity factors of sharp center V-notched tensile configuration using strain gauge technique

Pranjol Paul, K.S.R. Krishna Murthy, Debabrata Chakraborty

DOI: [10.1504/IJCMSSE.2023.10059844](https://doi.org/10.1504/IJCMSSE.2023.10059844)

Article History:

Received:	06 February 2023
Last revised:	05 July 2023
Accepted:	28 August 2023
Published online:	08 January 2024

A finite element simulation for notch stress intensity factors of sharp center V-notched tensile configuration using strain gauge technique

Pranjol Paul*, K.S.R. Krishna Murthy and
Debabrata Chakraborty

Department of Mechanical Engineering,
IIT Guwahati,
Guwahati, 781039, Assam, India
Email: pranjol@iitg.ac.in
Email: ksrkm@iitg.ac.in
Email: chakra@iitg.ac.in

*Corresponding author

Abstract: The present paper aims at theoretical development of a strain gauge-based methodology for accurate determination of notch stress intensity factor (NSIF) in sharp center V-notched tensile configuration (CENT). In line with Dally-Sanford's single strain gauge technique for determination of stress intensity factor (SIF) in cracked configuration, theoretical formulations have first been developed for single edge notch tensile (SENT) specimen and the same is applied to CENT by making necessary changes. Efficacy of the theoretical formulations developed has been investigated by carrying out finite element (FE) simulation in extracting NSIF for CENT. Results from FE simulations show that the theoretical formulations developed could correctly guide in accurate extraction of NSIF from the strain gauge readings in the case of CENT. In addition, it was also observed that the bounds on the strain gauge location put forward by the present formulation has an important bearing on accuracy of extracted NSIF. Placing strain gauges within and outside the upper bound results in highly accurate (<5%) and highly erroneous (>30%) values of NSIF respectively.

Keywords: sharp center V-notch; NSIF; notch stress intensity factor; strain gauge technique; mode I; optimal radial strain gauge location.

Reference to this paper should be made as follows: Paul, P., Krishna Murthy, K.S.R. and Chakraborty, D. (2023) 'A finite element simulation for notch stress intensity factors of sharp center V-notched tensile configuration using strain gauge technique', *Int. J. Computational Materials Science and Surface Engineering*, Vol. 11, Nos. 3/4, pp.272–287.

Biographical notes: Pranjol Paul (BE, PhD [Pursuing]) is presently a PhD research scholar in the Department of Mechanical Engineering, Indian Institute of Technology Guwahati, India, under the joint supervision of Prof. K.S.R. Krishna Murthy and Prof. Debabrata Chakraborty. He is an Associate Member of Institution of Engineers (India) [IEI] and a Life Member of Indian Society of Theoretical and Applied Mechanics (ISTAM). Also, he is a Reviewer of *International Journal of Mechanical Engineering and Applications (IJMEA)*.

K.S.R. Krishna Murthy, PhD, is presently a Professor in the Department of Mechanical Engineering, Indian Institute of Technology Guwahati, India.

He is associated with professional bodies viz., The Society for Failure Analysis (SFA) and The Indian Structural Integrity Society (InSIS) as Life Member and has supervised several postgraduate and PhD dissertations. He works in the broad areas of error estimation, fracture and fatigue of metals. He is a Reviewer of several reputed SCI journals.

Debabrata Chakraborty, PhD, is presently a Professor in the Department of Mechanical Engineering, Indian Institute of Technology Guwahati, India. He is a Fellow of Institution of Engineers (India) [IEI] and has 30 years of experience in teaching and research in the broad area of applied mechanics and FRP composites structures in particular. He is a Reviewer of several reputed SCI journals.

This paper is a revised and expanded version of a paper entitled 'Mode-I notch stress intensity factors for sharp center V-notched tensile configuration using strain gage technique: a numerical assessment' presented at *ICAMCMME2022*, Hyderabad, 11–12 November, 2022.

1 Introduction

Notches in structural or machine components tend to reduce the load bearing capacity with time, prompt crack initiation leading to catastrophic failure of such components. Due to high stress concentration around sharp V-notches, it is important to calculate the notch stress intensity factors (NSIF) K^V . Seweryn (1994) found that when the NSIF reached the critical value, then a crack developed from a notch tip. Williams (1952), using eigen function expansion method, found that in a V-notch, the singularity occurs at the tip following $\sigma_{ij} = K^V r^{\lambda'-1} f_{ij}(\theta)$, where $\lambda'-1$ (the order of stress singularity) and $f_{ij}(\theta)$ (the angular function) are functions of γ (notch angle).

For a specific geometry of the specimen and the loading condition, the state of stress in the vicinity of the notch is completely defined by K^V similar to SIF for cracks. Researchers developed efficient numerical (Ayatollahi and Nejati, 2011; Gross and Mendelson, 1972; Hussain and Murthy, 2018; Kumar and Pandey, 2015; Li and Guo, 2001) and experimental (Prassianakis and Theocaris, 1980; Kondo et al., 2001; Kondo et al., 2014; Ayatollahi and Nejati, 2011; Ayatollahi et al., 2013) techniques for the determination of NSIF K^V for different notched configurations. Sarangi et al. (2010) developed a single strain gauge technique for cracks in isotropic materials for accurate determination of SIF. Chakraborty et al. (2016) developed a single strain gauge technique for accurate determination of mode I stress intensity factors in cracked orthotropic laminates.

Even though Paul et al. (2018) developed a finite element based single strain gauge technique to accurately determine NSIF K^V for single edge notch tensile (SENT) under mode I loading condition following Dally and Sanford (1987), no work is still reported for sharp center V-notch tensile configuration (CENT). In the present paper, thus, an attempt is made to apply the theories developed for SENT in determination of NSIF K^V

for CENT. With an objective to analyse whether the single strain gauge technique developed for SENT configuration could be applied to CENT configuration, first an FE based numerical methodology, supported by theoretical formulation, is discussed for CENT configuration. To understand the efficacy of the proposed methodology for analysing CENT, the FE simulated results are further validated with published results of Treifi et al. (2009).

2 Formulation details

Even though the fundamental approach for determination of K^V for CENT would be similar to that for SENT, the loaded boundary conditions would clearly distinguish between the CENT configuration and the SENT configuration. The complete procedure starting from the fundamental theoretical formulation till the implementation of proposed single strain gauge technique in CENT configurations are systematically presented in the following sub-sections.

2.1 Formulation for strain analysis of sharp center V-notches

It is assumed that a sharp center V-notched isotropic and homogeneous body is subjected to mode I loading (plane stress). According to Williams (1952), the stresses in polar coordinates (Figure 1) are represented by equation (1) as follows

$$\begin{Bmatrix} \sigma_r \\ \sigma_\theta \\ \tau_{r\theta} \end{Bmatrix} = \sum_{n=1}^{\infty} \text{Re} \left\{ \frac{\lambda'_n A'_n}{r^{1-\lambda'_n}} \begin{Bmatrix} (3-\lambda'_n)\cos(\lambda'_n-1)\theta + (\lambda'_n \cos 2\alpha + \cos 2\lambda'_n \alpha)\cos(\lambda'_n+1)\theta \\ (\lambda'_n+1)\cos(\lambda'_n-1)\theta - (\lambda'_n \cos 2\alpha + \cos 2\lambda'_n \alpha)\cos(\lambda'_n+1)\theta \\ (\lambda'_n-1)\sin(\lambda'_n-1)\theta - (\lambda'_n \cos 2\alpha + \cos 2\lambda'_n \alpha)\sin(\lambda'_n+1)\theta \end{Bmatrix} \right\} \quad (1)$$

In equation (1), n and A'_n represent the order of the terms and coefficients of terms respectively in Williams' infinite series and the corresponding eigen value for the mode I problems λ'_n . The eigen value λ'_n could be evaluated from the characteristic equation given by

$$\lambda'_n \sin 2\alpha + \sin 2\lambda'_n \alpha = 0 \quad (2)$$

Here, λ'_n the positive root of equation (2) defines the order of singularity beyond the notch tip for mode I loading and is dependent on α (equation (2)), and thus a function of γ (Figure 1). The eigenvalue λ'_n can be generally represented as

$$\lambda'_n = \lambda_n + i\lambda_n^* \quad (3)$$

The first eigenvalue λ'_1 has been observed to be always real meaning $\lambda'_1 = \lambda_1$ and $\lambda_1^* = 0$, but the higher order eigen values may be real or complex which is decided by the value of the notch angle. On the basis of the nature of notch eigenvalues (real or complex), the coefficients, A'_n in Williams expansion may be real or complex. Details about λ'_n and A'_n were illustrated earlier (Ayatollahi and Nejati, 2011; Paul et al., 2018). Therefore, the coefficients A'_n may be written as

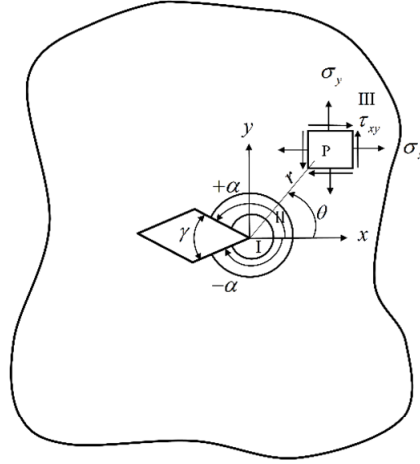
$$A'_n = A_n + iA_n^* \quad (4)$$

Since corresponding to $n = 1$, λ'_1 is real, $A'_1 = A_1$ is the only singular term and its relation to the NSIF K_I^V is

$$K_I^V = \lim_{r \rightarrow 0} (\sqrt{2\pi r^{1-\lambda'_1}} \sigma_y(\theta = 0)) = \sqrt{2\pi} \lambda'_1 (1 + \lambda'_1 - \lambda'_1 \cos 2\alpha - \cos 2\alpha \lambda'_1) A_1 \quad (5)$$

However, for $n > 1$, A'_n have both real and imaginary components.

Figure 1 Different zones (I, II and III) around a sharp center V notch tip



Using stress transformation, the Cartesian components of stresses (Figure 1) for mode I loading could be expressed as

$$\begin{Bmatrix} \sigma_x \\ \sigma_y \\ \tau_{xy} \end{Bmatrix} = \sum_{n=1}^{\infty} \text{Re} \left\{ \frac{\lambda'_n A'_n}{r^{1-\lambda'_n}} \begin{Bmatrix} (2 + \lambda'_n \cos 2\alpha + \cos 2\alpha \lambda'_n) \cos(\lambda'_n - 1)\theta - (\lambda'_n - 1) \cos(\lambda'_n - 3)\theta \\ (2 - \lambda'_n \cos 2\alpha - \cos 2\alpha \lambda'_n) \cos(\lambda'_n - 1)\theta + (\lambda'_n - 1) \cos(\lambda'_n - 3)\theta \\ -(\lambda'_n \cos 2\alpha + \cos 2\alpha \lambda'_n) \sin(\lambda'_n - 1)\theta + (\lambda'_n - 1) \sin(\lambda'_n - 3)\theta \end{Bmatrix} \right\} \quad (6)$$

Using the stress strain relations for plane state of stress, the strain components (ε_x , ε_y and γ_{xy}) at (r, θ)

$$\begin{aligned} 2G\varepsilon_x &= \sum_{n=1}^{\infty} \text{Re} \left\{ \frac{\lambda'_n A'_n}{r^{1-\lambda'_n}} \left[2\kappa \cos(\lambda'_n - 1)\theta + \lambda'_n \cdot \cos 2\alpha \cdot \cos(\lambda'_n - 1)\theta + \right. \right. \\ &\quad \left. \left. \cos 2\lambda'_n \alpha \cdot \cos(\lambda'_n - 1)\theta - (\lambda'_n - 1) \cdot \cos(\lambda'_n - 3)\theta \right] \right\} \\ 2G\varepsilon_y &= \sum_{n=1}^{\infty} \text{Re} \left\{ \frac{\lambda'_n A'_n}{r^{1-\lambda'_n}} \left[2\kappa \cos(\lambda'_n - 1)\theta - \lambda'_n \cdot \cos 2\alpha \cdot \cos(\lambda'_n - 1)\theta - \right. \right. \\ &\quad \left. \left. \cos 2\lambda'_n \alpha \cdot \cos(\lambda'_n - 1)\theta + (\lambda'_n - 1) \cdot \cos(\lambda'_n - 3)\theta \right] \right\} \\ 2G\gamma_{xy} &= \sum_{n=1}^{\infty} \text{Re} \left\{ \frac{\lambda'_n A'_n}{r^{1-\lambda'_n}} \left[2(\lambda'_n - 1) \cdot \sin(\lambda'_n - 3)\theta - \right. \right. \\ &\quad \left. \left. 2(\lambda'_n \cos 2\alpha + \cos 2\lambda'_n \alpha) \cdot \sin(\lambda'_n - 1)\theta \right] \right\} \end{aligned} \quad (7)$$

In equation (7), G is the rigidity modulus, for plane stress, $\kappa = (1-\nu)/(1+\nu)$ and for plane strain, $\kappa = 3-\nu$.

2.2 Formulation for single strain gauge technique

It is always essential to locate the strain gauges in a feasible zone ahead of the notch tip for accurate strain measurement. In Figure 1, the zone I lying close to the notch tip is not an optimal zone for precise strain measurement on account of plasticity, very stiff strain gradients and three dimensional stress state. The farthest zone in Figure 1 (zone III) also does not qualify as an optimal zone for strain measurement as the solutions exist in the form of infinite series leading to the requirement of large number of strain gauges. It is, therefore, concluded that a practically viable zone or an optimal region for measuring such surface strains is zone II. In zone II, the strains are assumed to comprise a singular term (the first term of the infinite series) and additional one or two higher order terms (specifically second order) which are non-singular according to Williams (1952). In zone II, the components of strain with terms associated with $n=1$ and $n=2$ are generalised as

$$\begin{aligned}
 2G\epsilon_x &= r^{\lambda_1-1} A_1 g_1^x(\lambda_1, \nu, \theta, \gamma) + r^{\lambda_2-1} A_2 g_2^x(r, \lambda_2^*, \lambda_2, \theta, \gamma, \nu) + r^{\lambda_2-1} A_2^* g_2^{x*}(r, \lambda_2^*, \lambda_2, \theta, \gamma, \nu) \\
 2G\epsilon_y &= r^{\lambda_1-1} A_1 g_1^y(\lambda_1, \nu, \theta, \gamma) + r^{\lambda_2-1} A_2 g_2^y(r, \lambda_2^*, \lambda_2, \theta, \gamma, \nu) + r^{\lambda_2-1} A_2^* g_2^{y*}(r, \lambda_2^*, \lambda_2, \theta, \gamma, \nu) \\
 2G\gamma_{xy} &= r^{\lambda_1-1} A_1 g_1^{xy}(\lambda_1, \theta, \gamma) + r^{\lambda_2+1} A_2 g_2^{xy}(r, \lambda_2^*, \lambda_2, \theta, \gamma) + r^{\lambda_2+1} A_2^* g_2^{xy*}(r, \lambda_2^*, \lambda_2, \theta, \gamma)
 \end{aligned}
 \tag{8}$$

The strain expressions in equation (7) are reduced to equation (8) containing only three unknown coefficients A_1 , A_2 and A_2^* for a given notched configuration. The strain expressions, as seen in equation (8), consist of a singular term (the first order term) and two non-singular second order terms. The normal strain component (ϵ_a), at point P along ‘ a ’ which is subtending an angle β with the notch axis (Figure 2), is derived using strain transformation rule as

$$\begin{aligned}
 2G\epsilon_a &= r^{\lambda_1-1} A_1 f_1(\theta, \beta, \lambda_1, \nu, \gamma) + r^{\lambda_2-1} A_2 f_2(\theta, \beta, \lambda_2, \lambda_2^*, \gamma, \nu, r) \\
 &\quad + r^{\lambda_2-1} A_2^* f_2^*(\theta, \beta, \lambda_2, \lambda_2^*, \gamma, \nu, r)
 \end{aligned}
 \tag{9}$$

where the functions f_1 , f_2 and f_2^* were shown expanded by Paul et al. (2018). Using strain gauge readings from three radial locations, in equation (9), three simultaneous equations could be solved for A_1 , A_2 and A_2^* . After measuring A_1 , the parameter K_I^V (mode I NSIF) could be determined conveniently using equation (5).

Another simplified technique for measuring K_I^V using single strain gauge can be adopted by manipulating equation (9). According to this single strain gauge technique, the coefficient of the term A_2 in equation (9) should be equated to zero as follows

$$f_2(\theta, \beta, \lambda_2, \lambda_2^*, \gamma, \nu, r) = 0
 \tag{10}$$

and also the coefficient of the term A_2^* should be equated to zero as follows

$$f_2^*(\theta, \beta, \lambda_2, \lambda_2^*, \gamma, \nu, r) = 0 \tag{11}$$

It is observed that in the case of notch angle $\gamma \leq 40^\circ$ (approximately), λ_2' is real (i.e., $\lambda_2' = \lambda_2$) and thus λ_2^* vanishes resulting to $A_2^* = 0$ in equation (9). Thus, the resultant normal strain ϵ_a in equation (9) contains only the coefficients corresponding to A_1 and A_2 . Consequently, only the equation (10) should be satisfied in case of the notch angle $\gamma \leq 40^\circ$ and the equation (11) gets automatically satisfied because $\lambda_2^* = 0$ in such case. In case of $\gamma \leq 40^\circ$ and a specific Poisson's ratio ν , infinitely many combinations of θ and β can be obtained after solving equation (10). Finally for a particular combination of θ and β values, in case of $\gamma \leq 40^\circ$, equation (9) reduces to equation (12) (since $f_2 = 0$ and $f_2^* = 0$)

$$2G\epsilon_a = r^{\lambda_1 - 1} A_1 f_1(\theta, \beta, \lambda_1, \nu, \gamma) \tag{12}$$

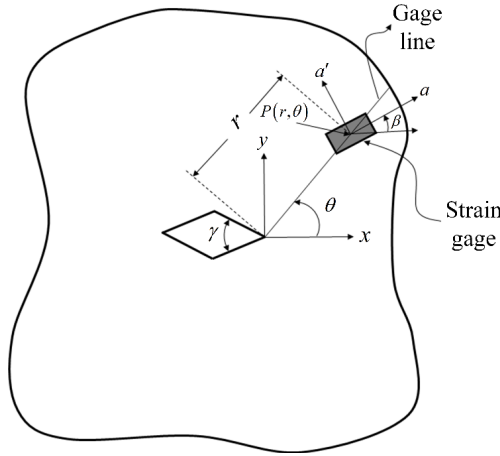
where

$$f_1(\theta, \beta, \lambda_1, \nu, \gamma) = \lambda_1 \left\{ \begin{array}{l} \cos^2 \beta [\cos \theta (\lambda_1 - 3) + \cos \theta (\lambda_1 - 1) [2\kappa + \cos \lambda_1 (2\pi - \gamma)]] - \\ \cos \theta (\lambda_1 - 3) \sin^2 \beta + 2\kappa \cos \theta (\lambda_1 - 1) \sin^2 \beta - \\ \cos \theta (\lambda_1 - 1) \cos \lambda_1 (2\pi - \gamma) \sin^2 \beta - \\ \sin \theta (\lambda_1 - 3) \sin 2\beta - \cos \lambda_1 (2\pi - \gamma) \sin \theta (\lambda_1 - 1) \sin 2\beta - \\ \lambda_1 \cos^2 \beta \cos \theta (\lambda_1 - 3) + \lambda_1 \cos^2 \beta \cos \gamma \cos \theta (\lambda_1 - 1) + \\ \lambda_1 \cos \theta (\lambda_1 - 3) \sin^2 \beta - \lambda_1 \cos \gamma \cos \theta (\lambda_1 - 1) \sin^2 \beta + \\ \lambda_1 \sin \theta (\lambda_1 - 3) \sin 2\beta - \lambda_1 \cos \gamma \sin \theta (\lambda_1 - 1) \sin 2\beta \end{array} \right\} \tag{13}$$

The equation (12) includes only A_1 meaning that only one strain gauge is required to determine A_1 . The schematic as shown in Figure 2 represents a point $P(r, \theta)$ on the gauge line characterised by θ at which the strain gauge needs to be positioned for strain measurement. At $P(r, \theta)$, the strain gauge is tilted along a direction making an angle β with notch axis (Figure 2). The measured strain ϵ_a at $P(r, \theta)$ will be substituted in equation (12) to evaluate A_1 . Subsequently, the mode I NSIF K_I^V is evaluated using equation (5).

In case of $\gamma > 40^\circ$, the equation (10) and equation (11) have to be simultaneously solved to get a unique combination of θ and β values for a particular Poisson's ratio ν . As λ_2^* does not vanish in case of $\gamma > 40^\circ$, thus ϵ_a in equation (9) comprises all the three coefficients A_1 , A_2 and A_2^* . With the unique combination of θ and β , the equation (9) will be reduced to equation (12) containing only coefficient A_1 to be determined. The procedure to determine K_I^V is same as discussed above for case $\gamma \leq 40^\circ$.

Figure 2 General schematic for strain gauge orientation in a sharp center V-notched body



2.3 Approximation of upper bound for the radial distance of strain gauge using finite element analysis

From equation (12), it can be observed that a prior knowledge of valid radial distance r is necessary for pasting the strain gauge in order to determine K_I^V . In order to accurately measure ϵ_a , the strain gauges need to be placed within the region where the multi-parameter strain series of equation (9) is valid, and this is the basic principle for estimation of optimal or valid strain gauge locations. In summary, the extent of validity of the selected strain series, equation (9), on the gauge line decides the magnitude of maximum permissible radial distance of strain gauge r_{max} within which the strain gauges ought to be pasted. Finite element analysis is carried out to determine the r_{max} which is discussed in the following paragraphs.

It is evident from equation (12) that the function f_1 is a constant. Other parameters such as rigidity modulus G and the Williams’ coefficient A_1 are also constants for a given notched configuration. Hence, equation (12) gets reduced to

$$\epsilon_a = \frac{C}{r^{1-\lambda_1}} \tag{14}$$

In equation (14), C is a constant. Applying logarithm on both sides in equation (14)

$$\ln \epsilon_a = (\lambda_1 - 1) \ln r + \ln C \tag{15}$$

The equation (15) is satisfied up to a radial distance $r \leq r_{max}$ from the tip of notch on the gauge line as shown in Figure 2. The equation (15) could be plotted as a graph between $\ln(\epsilon_a)$ vs. $\ln(r)$ representing a straight line with slope $(\lambda_1 - 1)$ and an intercept of $\ln(C)$. As $\lambda_1 < 1$, so the slope $(\lambda_1 - 1)$ is invariably negative. Ideally, the aforesaid straight line property will not be exhibited for radial distances $r > r_{max}$ on the gauge line as some more higher order Williams coefficients will be required in equation (9) in

addition to A_1 , A_2 and A_2^* to represent strain ϵ_a . Thus, for cases $r > r_{max}$, the equation (15) will no longer exhibit any straight line property. The r_{max} , thus, is the extent of radial location till which equation (12) is valid. In the present study, r_{max} has been determined by superimposing a straight line of slope $-(1-\lambda_1)$ on the plot between $\ln(\epsilon_a)$ and $\ln(r)$ and noticing the point where it deviates (Figure 3).

Figure 3 Plot of $\ln(\epsilon_a)$ vs. $\ln(r)$ along the gauge line

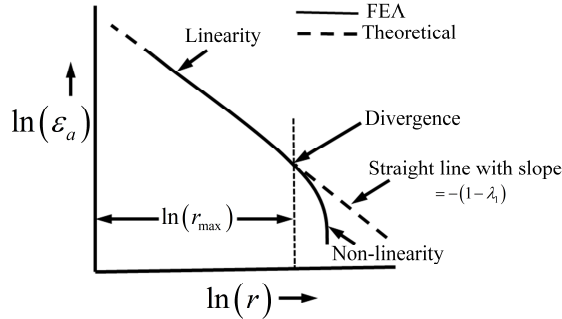


Figure 3 clearly shows that the r_{max} is literally the radial distance till which the graph between $\ln(\epsilon_a)$ and $\ln(r)$ exhibits the linear property but the graph begins exhibiting non-linear property beyond r_{max} . Once the value of r_{max} is established through the plot, then the optimal or valid radial strain gauge locations can be easily determined *a priori* using the equation as follows

$$r_{min} \leq r \leq r_{max} \tag{16}$$

where

$$r_{min} = 1.25 \times \text{plate thickness (Li and Guo, 2001)} \tag{17}$$

Any radial location r on the gauge line, if found satisfying equation (16), is an optimal or valid gauge location. Using finite element analysis, the strain ϵ_a is computed at a large number of nodes on the gauge line of a given sharp center V-notched configuration (i.e., from notch tip to the plate boundary).

3 Results and discussions

A sharp center V-notched plate under mode I loading with plane state of stress is considered as shown in the Figure 4. Geometry, material properties and loading parameters are listed in Table 1. Exploiting the symmetry of the specimen, only a quarter of the plate has been modelled in the FEA shown as shaded region in Figure 4 along with the boundary conditions. FEA has been carried out using general purpose FE software ANSYS and eight noded isoparametric elements (PLANE183) are used for meshing the analysis domain. Around the notch tip, eight noded elements have been collapsed in a characteristic spider web fashion. In order to understand the influence of notch angle on

the NSIF, four different notch angles viz., $0^\circ, 30^\circ, 45^\circ$ and 60° have been considered. In addition, four different a/b ratios viz., 0.2, 0.4, 0.6 and 0.8 have been considered to understand the influence of a/b ratio.

Figure 4 Sharp center V-notched configurations under uniaxial tension

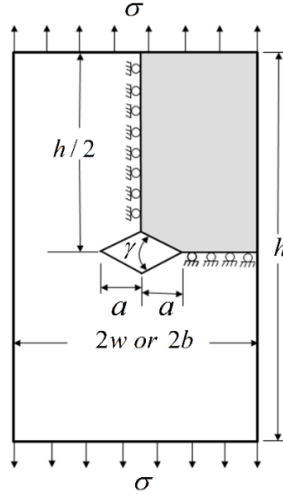
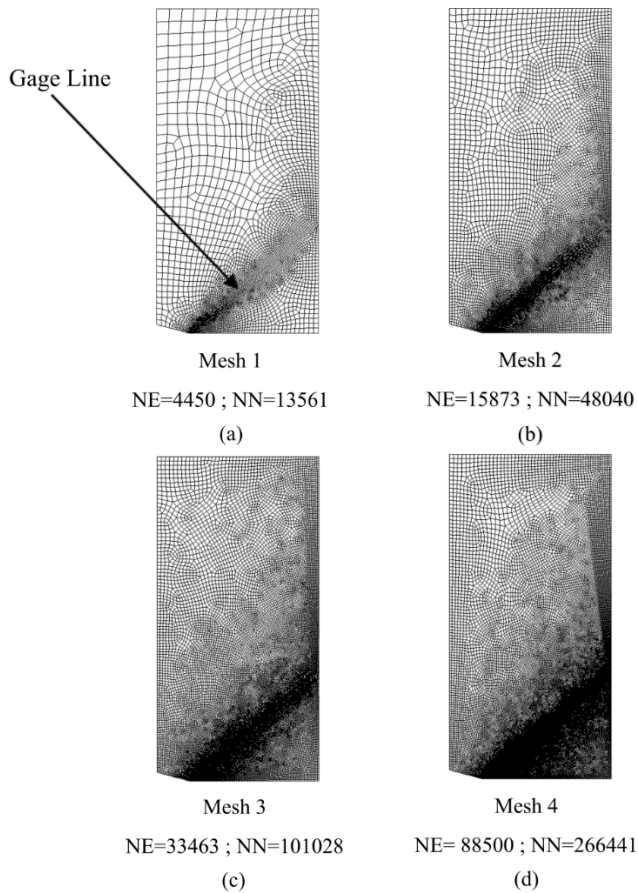


Table 1 Geometric, material and loading parameters of sharp center V-notched configurations

Example	b (mm)	Notch angle γ	a/b	$h/2b$	ν	E (GPa)	σ (MPa)
1	75	30°	0.2	2	1/3	200	100
2	75	$0^\circ, 30^\circ, 45^\circ, 60^\circ$	0.2, 0.4, 0.6, 0.8	2	1/3	200	100

3.1 Determination of r_{max} and mesh convergence

A mesh refinement study has been suitably carried out to decide the degree of refinement required in the present FEA based on the converged value of r_{max} . For this purpose, four meshes have been considered in the ascending order of mesh density with $a/b = 0.2$ as shown in Figure 5 indicating the number of elements (NE) and number of nodes (NN). The finite element meshes are so designed that a large number of nodes lie along a radial line known as the gauge line (Figure 5) making an angle of θ with the notch axis. This line emanates from the notch tip and spans up to the outer boundaries of the notched plate. From FEA, strains along the radial line are obtained in the global coordinate system and are transformed into the linear strain ϵ_a in the direction having an orientation of β with the notch axis. The radial distances (r) of each node from the notch tip along the gauge line are then obtained.

Figure 5 Mesh refinement for convergence: (a) Mesh 1; (b) Mesh 2; (c) Mesh 3 and (d) Mesh 4

As there is a necessity of knowing optimal or valid radial strain gauge locations to accurately measure the NSIF, so this gives rise to the necessity of knowing the appropriate range of radial distances within which the strain gauge can be pasted. The minimum permissible radial distance r_{\min} is 1.25 times the plate thickness and the maximum permissible radial distance r_{\max} is to be determined numerically using FEA. A plate thickness $t = 2$ mm has been considered in all the examples throughout, hence $r_{\min} = 1.25 \times 2$ mm = 2.5 mm. The log-log plot for each of the four meshes of the case $a/b = 0.2$ are shown in Figure 6 and the corresponding r_{\max} values are also shown. It is to be noted here that the notch tip point is not plotted as the radial distance r at this point is zero and the logarithm of zero is undefined. Each log-log plot (Figure 6) consists of very clear linear portion followed by a clear non-linear portion as stated in the previous section. The radial location corresponding to the terminal point of the linear portion of the plots in Figure 6 basically denotes the extent of the three parameter strain series or r_{\max} following equation (12). The extent of the linear portion of the plots (r_{\max}) is observed to gradually decrease with successive mesh refinement due to decreased finite

element size and convergence could be observed. Therefore, in all further analyses, the refined mesh (NE = 88500, NN = 266441) has been used. Table 2 shows the converged value as a result of mesh refinement study.

Figure 6 Plot of $\ln(\epsilon_a)$ vs. $\ln(r)$ for sharp center V-notch with $\gamma = 30^\circ$ subjected to mode I loading corresponding to four successive refined FE meshes viz.: (a) Mesh 1; (b) Mesh 2; (c) Mesh 3 and (d) Mesh 4 (see online version for colours)

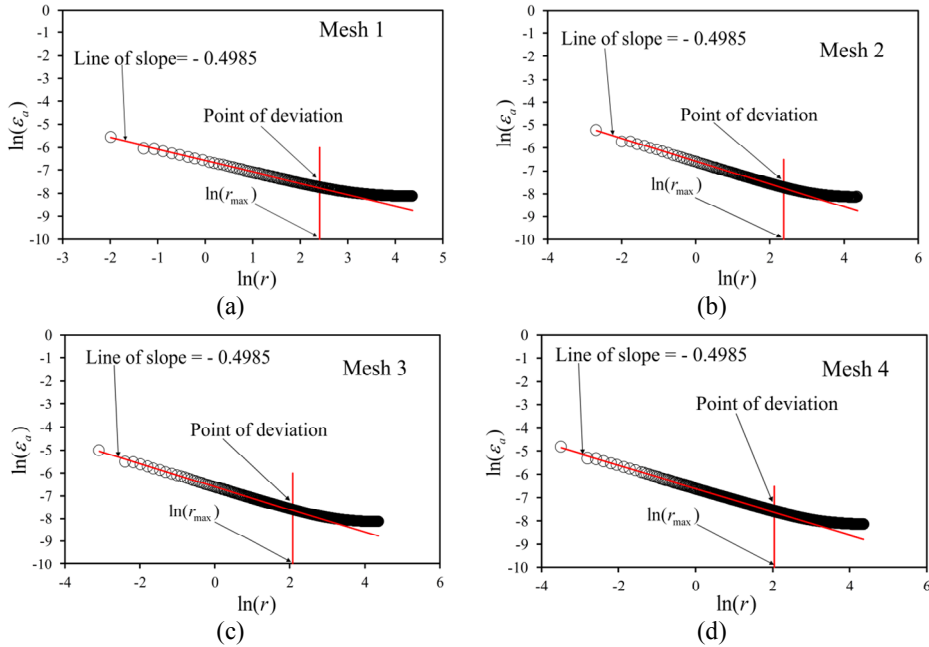
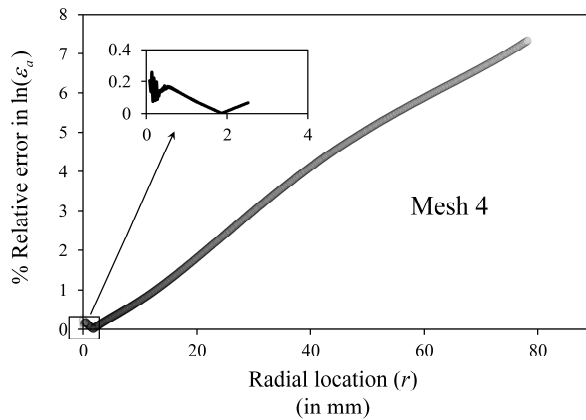


Table 2 Finite element mesh convergence for a sharp center V-notch with $\gamma = 30^\circ$, $a/b = 0.2$

Mesh	r_{max} (mm)
Mesh 1	11.13
Mesh 2	10.72
Mesh 3	7.98
Mesh 4	7.70

Figure 7 presents the relative error between the FE solution of Mesh 4 (Figure 5) and ideal solution of $\ln(\epsilon_a)$ (obtained from the straight line) at different radial locations along the gauge line. Figure 7 further shows that the error reduces monotonically when one observes from the non-linear portion to the linear portion. The radius where the error becomes less than 0.5% is regarded as the upper limit on the permissible radial distance (r_{max}) for pasting the strain gauge for the sharp centre V-notched configuration with $a/b = 0.2$ and notch angle $\gamma = 30^\circ$. The point representing the value of r_{max} is marked in all the log-log plots in Figure 6.

Figure 7 Relative error in the FE computed values of $\ln(\varepsilon_a)$ as a function of radial location along the gauge line of the sharp center V-notched configuration



3.2 Influence of a/b on r_{\max} in sharp center V-notched configurations

For any notched geometry, ascertaining the characteristic behaviour of the maximum permissible radial distance of strain gauge r_{\max} in response to the varying a/b ratio is very much essential. In this context, variation of r_{\max}/b with a/b ratio for sharp center V-notched configurations with different notch angles has been studied. Figure 8 shows the typical graph for the variation of $\ln(\varepsilon_a)$ with $\ln(r)$ for $a/b=0.2$ to 0.8 and $\gamma=60^\circ$ which is a direct representation of the determination of r_{\max} . It could be seen from Figure 8 that values of r_{\max} vary with the a/b ratio. In order to understand the influence of a/b ratio on r_{\max} , the ratio of r_{\max}/b is plotted against a/b for different notch angles as shown in Figure 9. Figure 9 exhibits the characteristic bell shaped curve showing that the parameter r_{\max}/b increases in the beginning while shifting from $a/b=0.2$ to $a/b=0.4$ and subsequently it decreases while shifting from $a/b=0.4$ to $a/b=0.8$ which is due to the edge effect as observed in the case of cracks as well as for SENT configurations (Sarangi et al., 2010; Paul et al., 2018). Figure 9 also gives an approximate trend of obtaining higher r_{\max} with higher notch angle γ at a constant a/b ratio.

Table 3 shows the r_{\max} values for different notch angles and corresponding to different a/b ratios considered in this study. More importantly, Table 3 shows the computed values of normalised notch SIF and their comparison with the reference solutions (Treifi et al., 2009). As could be seen from Table 3 that the normalised notch SIF for all the cases of notch angles and a/b considered in the present study show excellent agreement with the reference solution with highest error being only 1.87%. This clearly shows that theoretical developments for determination of notch SIF using single strain gauge leads to correct values of K^V when implemented numerically. This

reinforces that the single strain gauge technique developed for SENT could be applied to CENT for determination of notch SIF.

Figure 8 Plot of $\ln(\epsilon_a)$ vs. $\ln(r)$ for mode-I sharp center V-notched configurations with notch angle $\gamma = 60^\circ$ (see online version for colours)

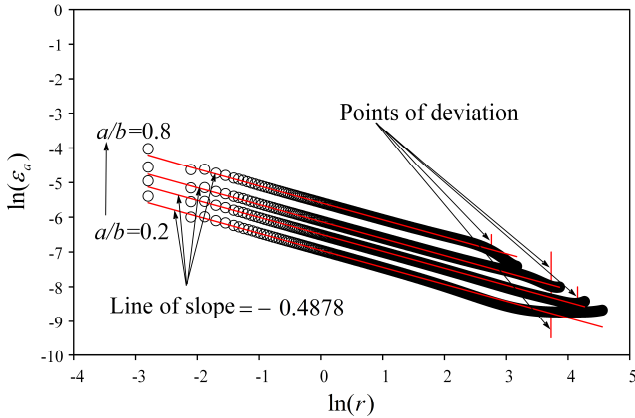
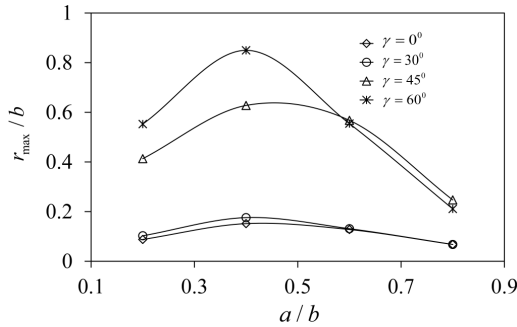


Figure 9 r_{\max} / b variation with a / b for sharp center V-notched configuration for different notch angles γ under mode I loading condition



In addition to showing the trends of r_{\max} with a / b and notch angle as discussed, results in Table 3 also show that notch SIF increases with increasing notch angles from 0° to 60° for all a / b ratios. In order to substantiate the usefulness of knowing r_{\max} *a priori*, strain measurements are taken at selected optimal and non-optimal radial gauge locations and NSIFs are calculated based on those strain values and listed in Table 4. Table 4 clearly shows that the notch SIF values show excellent agreement with the reference solution at radial locations $r < r_{\max}$, the percentage relative error increases at radial locations $r > r_{\max}$, and the error is as high as 30% at r which is far ahead of r_{\max} . Though the results in Table 4 correspond to $\gamma = 30^\circ$ and $a / b = 0.2$ particularly, however the trends for other a / b and γ were observed to be the same. This again clearly substantiates the importance of r_{\max} in accurate determination of notch SIF in CENT specimen.

Table 3 Validation of computed results (notch stress intensity factors) with published results

Notch angle γ	a / b	r_{\max} (mm)	Normalised	Normalised	Error % in normalised NSIF
			NSIF $\frac{K_I^V}{\sigma\sqrt{\pi a^{1-\lambda_1}}}$	NSIF (Treifi et al., 2009)	
0°	0.2	6.59	1.031	1.024	0.68
	0.4	11.37	1.110	1.109	0.09
	0.6	9.59	1.311	1.303	0.61
	0.8	5.07	1.812	1.814	0.11
30°	0.2	7.70	1.070	1.053	1.61
	0.4	13.19	1.160	1.151	0.78
	0.6	9.84	1.378	1.375	0.22
	0.8	5.08	1.971	1.959	0.61
45°	0.2	30.99	1.087	1.067	1.87
	0.4	47.07	1.197	1.184	1.09
	0.6	42.57	1.442	1.433	0.63
	0.8	18.53	2.093	2.072	1.01
60°	0.2	41.44	1.138	1.131	0.62
	0.4	63.72	1.265	1.261	0.32
	0.6	41.58	1.560	1.547	0.84
	0.8	15.81	2.2826	2.283	0.02

Source: Treifi et al. (2009)

Table 4 Error in mode-I normalised NSIF, K_I^V at different strain gauge locations for sharp center V-notch with $\gamma = 30^\circ$, $a / b = 0.2$ ($r_{\max} = 7.7$ mm, $r_{\min} = 2.5$ mm)

Radial location (in mm), r	r / r_{\max}	Estimated normalised K_I^V	% Relative error (Normalised $K_{I-Ref}^V = 1.053$)
3.0 (optimal)	0.38961	1.080	2.6
4.0 (optimal)	0.519481	1.087	3.2
5.0 (optimal)	0.649351	1.093	3.8
6.0 (optimal)	0.779221	1.101	4.6
7.0 (optimal)	0.909091	1.108	5.2
8.0 (Non optimal)	1.038961	1.115	5.9
9.0 (Non optimal)	1.168831	1.124	6.7
11.0 (Non optimal)	1.428571	1.140	8.3
15.0 (Non optimal)	1.948052	1.179	12.0
20.0 (Non optimal)	2.597403	1.238	17.6
25.0 (Non optimal)	3.246753	1.303	23.7
30.0 (Non optimal)	3.896104	1.374	30.5

4 Conclusion

The presented work shows theoretical formulations for CENT configuration followed by FE simulations for determination of accurate NSIF based on Williams' strain series expansion approach and Dally-Sanford's single strain gauge technique. We could observe that the theoretical formulations developed for determination of accurate NSIF for SENT using a single strain gauge technique could be also used for determination of accurate NSIF for CENT and examining the versatility of these formulations with CENT configurations is purely a novel research work. In addition, the presented work shows the importance of optimal or valid radial strain gauge locations for obtaining accurate NSIFs. There exists a maximum permissible radial distance r_{\max} within which the strain gauge needs to be pasted to ensure determination of accurate NSIF. For a given CENT configuration, the r_{\max} could be determined *a priori* using the proposed finite element based methodology and it varies with a/b ratio of CENT for a given notch angle. With the increase in a/b , r_{\max} increases up to a certain value of a/b , and beyond that r_{\max} again decreases exhibiting a characteristic bell shaped curve. Numerical (finite element) simulations show that in determination of accurate NSIF for CENT configurations using the proposed single strain gauge technique, a highly accurate (error < 3%) value of NSIF may be obtained only if the strain is measured within r_{\max} , but a highly erroneous (error > 30%) NSIF may result if strain is measured beyond r_{\max} . With the help of the present investigation, we could conclude that the NSIF, in CENT configurations, increases with notch angle and a/b ratio.

References

- Ayatollahi, M.R. and Nejati, M. (2011) 'Determination of NSIFs and coefficients of higher order terms for sharp notches using finite element method', *International Journal of Mechanical Sciences*, Vol. 53, pp.164–177.
- Ayatollahi, M.R. and Nejati, M. (2011) 'Experimental evaluation of stress field around the sharp notches using photoelasticity', *Materials and Design*, Vol. 32, pp.561–569.
- Ayatollahi, M.R., Dehghany, M. and Mirsayar, M.M. (2013) 'A comprehensive photoelastic study for mode I sharp V-notches', *European Journal of Mechanics – A/Solids*, Vol. 37, pp.216–230.
- Chakraborty, D., Murthy, K.S.R.K. and Chakraborty, D. (2016) 'Determination of K_I in orthotropic laminates with double ended cracks using a single strain gage technique', *Theoretical and Applied Fracture Mechanics*, Vol. 82, pp.96–106.
- Dally, J.W. and Sanford, R.J. (1987) 'Strain-gage methods for measuring the opening-mode stress-intensity Factor, K_I ', *Experimental Mechanics*, Vol. 27, pp.381–388.
- Gross, B. and Mendelson, A. (1972) 'Plane elastostatic analysis of V-notched plates', *International Journal of Fracture Mechanics*, Vol. 8, pp.267–276.
- Hussain, M.K. and Murthy, K.S.R.K. (2018) 'A point substitution displacement technique for estimation of elastic notch stress intensities of sharp V-notched bodies', *Theoretical and Applied Fracture Mechanics*, Vol. 97, pp.87–97.
- Kondo, T., Kobayashi, M. and Sekine, H. (2001) 'Strain gage method for determining stress intensities of sharp-notched strips', *Experimental Mechanics*, Vol. 41, pp.1–7.

- Kondo, T., Kurabe, Y., Sasaki, T., Kurahashi, T. and Miyashita, Y. (2014) 'Use of strain gages for determining generalized stress intensity factors of sharp V-notched plates under transverse bending', *Engineering Fracture Mechanics*, Vols. 124–125, pp.248–261.
- Kumar, D. and Pandey, K.N. (2015) 'A finite element simulation of the stress intensity factors in a plate with pre-cracked edge before and after coatings subjected to thermal loading', *International Journal of Computational Materials Science and Surface Engineering*, Vol. 6, No. 2, pp.75–96.
- Li, Z. and Guo, W. (2001) 'Three-dimensional elastic stress fields ahead of blunt V-notches in finite thickness plates', *International Journal of Fracture Mechanics*, Vol. 107, pp.53–71.
- Paul, P., Murthy, K.S.R.K. and Chakraborty, D. (2018) 'A strain gage technique for mode I notch stress intensity factor of sharp V-notched configurations', *Theoretical and Applied Fracture Mechanics*, Vol. 94, pp.57–70.
- Prassianakis, J.N. and Theocaris, P.S. (1980) 'Stress intensity factors at V-notched elastic, symmetrically loaded, plates by the method of caustics', *Journal of Physics D: Applied Physics*, Vol. 13, pp.1043–1053.
- Sarangi, H., Murthy, K.S.R.K. and Chakraborty, D. (2010) 'Radial locations of strain gages for accurate measurement of mode I stress intensity factor', *Materials and Design*, Vol. 31, pp.2840–2850.
- Seweryn, A. (1994) 'Brittle fracture criterion for structures with sharp notches', *Engineering Fracture Mechanics*, Vol. 47, No. 5, pp.673–681.
- Treif, M., Oyadiji, S.O. and Tsang, D.K.L. (2009) 'Computations of the stress intensity factors of double-edge and centre V-notched plates under tension and anti-plane shear by the fractal-like finite element method', *Engineering Fracture Mechanics*, Vol. 76, pp.2091–2108.
- Williams, M.L. (1952) 'Stress singularities resulting from various boundary conditions in angular corners of plates in extension', *Journal of Applied Mechanics*, Vol. 19, No. 4, pp.526–528.